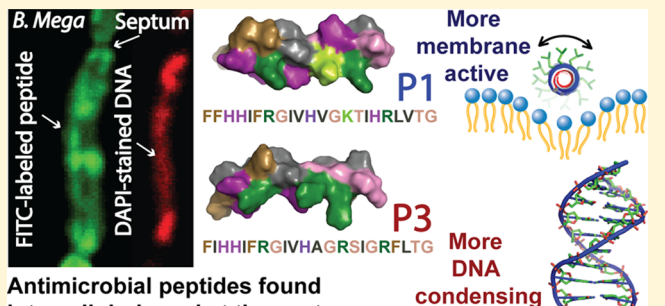


Complementary Effects of Host Defense Peptides Piscidin 1 and Piscidin 3 on DNA and Lipid Membranes: Biophysical Insights into **Contrasting Biological Activities**

Robert M. Hayden, [†] Gina K. Goldberg, [†] Bryan M. Ferguson, [†] Mason W. Schoeneck, [†] M. Daben J. Libardo, [‡] Sophie E. Mayeux, [†] Akritee Shrestha, [†] Kimberly A. Bogardus, [†] Janet Hammer, [§] Sergey Pryshchep, ^{||} Herman K. Lehman, [†] Michael L. McCormick, [†] Jack Blazyk, [§] Alfredo M. Angeles-Boza, Rigiang Fu, and Myriam L. Cotten*

Supporting Information

ABSTRACT: Piscidins were the first antimicrobial peptides discovered in the mast cells of vertebrates. While two family members, piscidin 1 (p1) and piscidin 3 (p3), have highly similar sequences and α -helical structures when bound to model membranes, p1 generally exhibits stronger antimicrobial and hemolytic activity than p3 for reasons that remain elusive. In this study, we combine activity assays and biophysical methods to investigate the mechanisms underlying the cellular function and differing biological potencies of these peptides, and report findings spanning three major facets. First, added to Gram-positive (Bacillus megaterium) and Gram-negative (Escherichia coli) bacteria at sublethal concentrations and



Antimicrobial peptides found intracellularly and at the septa

imaged by confocal microscopy, both p1 and p3 translocate across cell membranes and colocalize with nucleoids. In E. coli, translocation is accompanied by nonlethal permeabilization that features more pronounced leakage for p1. Second, p1 is also more disruptive than p3 to bacterial model membranes, as quantified by a dye-leakage assay and ²H solid-state NMR-monitored lipid acyl chain order parameters. Oriented CD studies in the same bilayers show that, beyond a critical peptide concentration, both peptides transition from a surface-bound state to a tilted orientation. Third, gel retardation experiments and CD-monitored titrations on isolated DNA demonstrate that both peptides bind DNA but p3 has stronger condensing effects. Notably, solid-state NMR reveals that the peptides are α -helical when bound to DNA. Overall, these studies identify two polyreactive piscidin isoforms that bind phosphate-containing targets in a poised amphipathic α -helical conformation, disrupt bacterial membranes, and access the intracellular constituents of target cells. Remarkably, the two isoforms have complementary effects; p1 is more membrane active, while p3 has stronger DNA-condensing effects. Subtle differences in their physicochemical properties are highlighted to help explain their contrasting activities.

INTRODUCTION

As key participants in innate immunity, cationic antimicrobial peptides (AMPs) are multifunctional host defense molecules that can be expressed constitutively or induced by pathogens and danger signals.¹⁻⁴ AMPs were originally described as providing a first line of defense against a wide range of microbes that they can directly eradicate via membrane lysis or intracellular targeting.²⁻⁴ In recent years, their new characterization as host defense peptides (HDPs), rather than AMPs, has emerged to reflect their multifaceted functions on host cells,

including the immunomodulatory, anti-inflammatory, and wound-healing effects they manifest under physiological conditions. 1,3,5 Since some HDPs activate adaptive immune cells (e.g., T-lymphocytes) as well as cells that link the adaptive and innate immune systems (e.g., dendritic cells, macrophages), they are also considered to be important participants in the

October 3, 2015 Received: Revised: November 14, 2015 Published: November 16, 2015

[†]Department of Chemistry, Hamilton College, Clinton, New York 13323, United States

Department of Chemistry, University of Connecticut, Storrs, Connecticut 06269, United States

Department of Biomedical Sciences, Ohio University, Athens, Ohio 45701, United States

Center for Biotechnology and Interdisciplinary Studies, Rensselaer Polytechnic Institute, Troy, New York 12180, United States

¹Department of Biology, Hamilton College, Clinton, New York 13323, United States

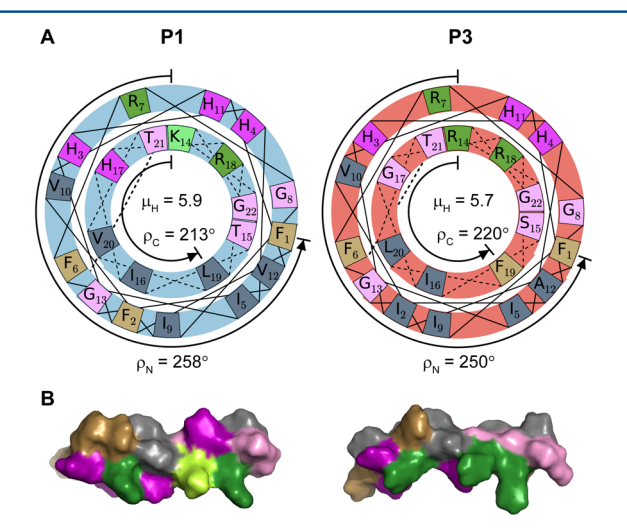
^{*}National High Magnetic Field Laboratory, Tallahassee, Florida 32310, United States

interplay between adaptive and innate immunities. 5 While any given HDP can be multifunctional, organisms rely on a plethora of HDPs that can act synergistically to boost the immune response of the host and combat infections. 3,5,6 In light of their anti-infective potencies, low inductance of bacterial resistance, synergistic effects with conventional antibiotics, and protection of the host from antibiotic-induced septic shock and overactive inflammatory response, HDPs have garnered significant interest in terms of development of new therapeutics effective against multidrug resistant bacteria, which represent a growing public health threat worldwide. 1-3,6-8

Since AMPs play multifaceted roles in immunity, it is not surprising that they are often intrinsically disordered molecules and exhibit conformational plasticity. Biophysically, this variety translates into versatile modes of interaction that could underpin multispecificity and polyreactivity, and therefore multihit mechanisms and broad-spectrum activity. While their mechanisms of action as AMPs (i.e., direct antimicrobial agents) are not fully understood on a molecular level, cationic HDPs are known to initially rely on electrostatic interactions to recognize and interact with microbial cell membranes. 2,4,9 Bacterial cell death may then be achieved through disruption of the essential cell membrane and/or translocation across this membrane to reach and disrupt vital intracellular targets (e.g., DNA; RNA; protein synthesis and folding; enzymatic functions). 3,5,6,10,11 However, it is not known how various factors such as the concentration and physicochemical features (e.g., hydrophobicity, charge, amphipathicity, angle subtended by the polar residues) of the peptides influence the relative contribution of membrane disruptive and intracellular effects to their mechanisms of cell death. As a result, even though a number of well-studied HDPs have been shown to penetrate bacterial membranes, a direct causal relationship between intracellular effects and the lethal step has been established for only a few. 12,13 Understanding the physicochemical principles underlying the mechanisms of action of the most potent AMPs and comparing them to other membrane-disruptive or translocating peptides such as cell penetrating peptides (CPPs) and preamyloid toxins (PATs) that are also amphipathic and cationic are necessary steps to rationally design drugs with improved therapeutic effects, lower toxicity, and enhanced stability in vivo.

Members of the piscidin family were the first AMPs discovered in the mast cells of vertebrates. 14,15 An important consequence of this finding was intensified research that revealed the crucial role of AMPs and mast cells in the first line of defense against infectious diseases. 16,17 Originally isolated from the hybrid striped seabass, piscidin 1 (p1: FFHHIFRG-IVHVGKTIHRLVTG) and piscidin 3 (p3: FIHHIFRGIVHA-GRSIGRFLTG) are 22-residue-long, cationic, amphipathic, and membrane disruptive isoforms from the piscidin family. 14,15,18-20 Similar to other piscidins, p1 and p3 feature an unusually high content of histidine residues (20% in p1 versus 2% on average in the >2500 peptides deposited in the AMP database). 19 Notably, p1 and ascaphin-8 are the only AMPs known to combine broad-spectrum antimicrobial activity on both Gram-positive and Gram-negative bacteria as well as anti-HIV-1 and anticancer properties. 19,20 Apponyi et al. recently reviewed highly potent antimicrobial frog peptides and highlighted that caerin 1.1 is also anticancer and anti-HIV but its antimicrobial activity is mostly focused on Gram-positive bacteria.²¹ Recently, p1 and tilapia p3 (TP3) were shown to have HDP functions, including anti-inflammatory properties

not only in vitro (macrophages)²² but also in vivo (mice),²³ and p1 was shown to be an anesthetic.²⁴ While both peptides have highly similar amino acid sequences and therefore physicochemical properties (Figure 1), and demonstrate comparable



FFHHIFRGIVHVGKTIHRLVTG FIHHIFRGIVHAGRSIGRFLTG

Figure 1. (A) Helical wheel diagrams for p1 (left) and p3 (right) as determined by solid-state NMR in 1:1 POPE/POPG. 26 Kinking is manifested by rotation angles about the helical axis that are different for the N-end $(\rho_{\rm N})$ and C-end $(\rho_{\rm C})$ on each side of Gly13. The hydrophobic moment (μ_H) calculated as explained previously²⁶ is specified. (B) Surface rendering of the peptide 3D structures in 1:1 POPE/POPG. The color scheme is as indicated in the amino sequences. Notably, His17 (purple, top right corner) in p1 is at the interface between the hydrophilic and hydrophobic section, while in p3 this residue is a flexible glycine. Other distinctions include the presence of three arginines and four glycines in p3 while p1 has two and three of them, respectively. PDB ID: 2MCV (p1) and 2MCX

potency against Gram-positive bacteria, p1 is more hemolytic and usually more active than p3 against Gram-negative bacteria for reasons that remain elusive. 15,25,26 Bound to bacterial mimetic lipid bilayers, p1 and p3 adopt disrupted α -helical conformations that kink in the middle at a highly conserved glycine to optimize contacts with the hydrophobic core of the bilayer (Figure 1).²⁶ Distinctions between the amphipathicity of the helical structures of p1 and p3 (Figure 1) correlate with differences in their antimicrobial potency and support an interfacial activity mode of action where peptide carpeting on the membrane surface followed by insertion in the bilayer leads to loss of segregation between the polar and nonpolar regions of the bilayer, and creates packing defects in the bilayer and/or disordered toroidal pores through which leakage can occur. 9,26

While the membrane-binding and -disrupting properties of p1 and p3 have been documented, 22,25-31 the possibility that they translocate across bacterial cell membranes, and have other targets than membranes as part of their mechanisms of cell death, is plausible for several reasons. First, piscidin has physicochemical properties that CPPs and translocating AMPs also share, including cationicity, amphipathicity, patches of cationic residues, and a high content of one or two selected amino acids (Arg, Lys, Trp, His). 10,12,32,33 In this regard, the high histidine content of p1 and p3 may confer an advantage in translocating across membranes as pH-sensitive cargo-complexed peptides that can deliver DNA intracellularly.³⁴ Second,

because the ability to translocate is not shared by all AMPs, it has been suggested that this property is restricted to only some peptide families. This is a significant observation for piscidins because pleurocidins, which are part of the piscidin family, translocate across *E. coli* membranes below their minimum inhibitory concentrations (MICs) and disrupt the synthesis of macromolecules. The suggestion of the property of th

Focusing on the two piscidin family members, p1 and p3, this study combines multiple biochemical and biophysical methods to investigate their mode of action as AMPs that act directly on bacterial cells. The investigations, which are strongly motivated by the search for molecular drivers and physicochemical parameters underpinning the contrasting biological activities of these two natural peptides, characterize their relative abilities to affect biological membranes and DNA. Using confocal microscopy, we studied the ability of p1 and p3 to translocate across Gram-positive and Gram-negative bacterial membranes below their MICs and colocalize with nucleoids. Inner membrane (IM) permeabilization of live E. coli was used to investigate if both peptides could permeabilize cells at sublethal concentrations. Studies executed with model membranes and isolated DNA were performed to better understand peptide translocation and interactions with these cellular components. Using 1:1 1-palmitoyl-2-oleoyl-sn-glycero-3-phosphatidylethanolamine/palmitoyl-2-oleoyl-sn-glycero-3-phosphoglycerol (POPE/POPG) as bacterial model membranes, we obtained dye leakage assay data on large unilamellar vesicles (LUVs) to confirm that the model membranes reflected the relative membrane disruptive potencies of p1 and p3 on bacteria. Solidstate NMR was then performed to measure lipid acyl chain order parameters of 1:1 POPE/POPG-d31 in the presence of p1 versus p3. Oriented CD was also carried out in these model bilayers to study the ability of p1 and p3 to change from a surface-bound state at low peptide-to-lipid ratio (P/L) to a tilted state at higher P/L, and therefore identify a possible molecular model for membrane activity and translocation. Gel retardation assays and CD-monitored titrations performed using isolated DNA were accomplished to characterize the ability of p1 and p3 to retard and condense DNA, while solidstate NMR distance measurements were carried out to characterize the secondary structure of the peptides bound to DNA. Overall, this study provides insights that may be helpful in not only better understanding the polydiversity of piscidins and related AMPs but also identifying important physicochemical features of histidine-rich peptides to further develop antiinfective drugs and gene therapies. The investigation also provides an opportunity to examine whether, as peptides evolve to have stronger disruptive effects on phospholipid bilayers, they congruently have weaker effects on DNA, another phosphate-containing target.

EXPERIMENTAL METHODS

Materials, Peptide Synthesis, and Purification. Chemicals were obtained from Sigma-Aldrich (Saint Louis, MO) unless otherwise indicated. Carboxyamidated p1 (MW 2571) and p3 (MW 2492) were synthesized by solid-phase peptide synthesis at the University of Texas Southwestern Medical Center and purified by HPLC as previously described. For the fluorescein isothiocyanate (FITC) forms of the peptides, the fluorescein label was attached to the amino end of the peptides before cleavage from the resin. The peptides were washed with dilute HCl and dialyzed to remove residual trifluoroacetic acid (TFA; Sigma-Aldrich), leading to 98% pure

peptides. Their concentrations were obtained by amino acid analysis at the Protein Chemistry Center at Texas A&M.

Antimicrobial Assays. MIC values were obtained using the method outlined by Chekmenev et al.²⁵ and briefly outlined in the Supporting Information.

Confocal Microscopy. Mid-logarithmic phase *E. coli* and *B.* megaterium were treated first with 0.75 µM FITC-p1 or FITCp3 for 30 min and second with 0.75 nM 4',6-diamidino-2phenylindole (DAPI) (Life Technologies) for another 30 min prior to washing with 10 mM PBS (Fisher BioReagents). Next, they were fixed with 4% paraformaldehyde (in phosphate buffer), immobilized on poly-L-lysine-coated #1.5 circular coverslips, and mounted with 100% glycerol. Imaging was performed by sequential scanning of FITC-piscidin (green) and DAPI-stained DNA (blue but pseudocolored red to enhance contrast) on a Zeiss LSM 510 Meta/Multiphoton NLO microscope using a 100×/1.4 oil-immersion lens at the Center for Biotechnology and Interdisciplinary Studies at RPI (Troy, NY). FITC-piscidin was detected at LP505 nm emission after excitation with a 488 nm argon laser, while DAPI was excited via a Ti:sapphire laser (Coherent Chameleon) at 720 nm and detected with a bandpass filter between 390 and 465 nm. Under these conditions, bleedthrough of the FITC signal into the DAPI channel was avoided. Contrast enhancement was employed to improve the visibility of the bright field images. By itself, fluorescein is known to be cell impermeant; controls run under the experimental conditions described here confirmed that it was the case.

Permeabilization Experiments. Permeabilization assays on live bacteria involved following the cleavage of the lactose analogue ortho-nitrophenyl- β -galactoside (ONPG) into *o*-nitrophenol (ONP) by β -galactosidase constitutively expressed by the ML-35 strain of *E. coli*, which is deficient in lactose permease.³⁸ The standard protocol is briefly described in the Supporting Information.

Calcein Leakage Experiments. Calcein-loaded large unilamellar vesicles (LUVs) were exposed to p1 and p3 to determine the ability of the peptides to cause leakage. A standard protocol was followed and outlined in the Supporting Information.

Gel Retardation Assays. A 5 μ L aliquot (100 ng) of the linearized plasmid pNEB206A (2706 bp; New England Biolabs, Ipswich, MA) was incubated with increasing amounts of peptide (0–800 ng from a 100 ng/ μ L stock) for 30 min. The total volume was maintained at 15 μ L by adding appropriate amounts of 10 mM PBS at pH 7.4. After addition of loading dye, the samples were placed into a 1% agarose gel and run at 120 V for 90 min. The DNA was visualized by staining with ethidium bromide (75 μ g/L) for 15 min followed by destaining with nanopure water for 10 min. Gels were imaged using a Bio-Rad Gel-Doc XR+, and bands were quantified using the accompanying Image Lab 5.0 software. EC₅₀ and EC₉₀ values of DNA retardation were calculated from a best-fit line using values obtained from three independent experiments.

Circular Dichroism. Titrations of duplex DNA (AAAT-ACACTTTTGGT, MW 9141.1; Integrated DNA Technologies) by p1 and p3 were performed in Tris buffer (10 mM Tris, pH 7.5, 0.1 mM EDTA) at a DNA concentration of 2.0 μ M using a previously published protocol and briefly explained in the Supporting Information.³⁹

Oriented Circular Dichroism. Lipids (approximately 0.5 mg) dissolved in chloroform were added to a desired amount of peptide in 2,2,2-trifluoroethanol (TFE, Acros Organics). The

organic solvents were dried under a flow of nitrogen and placed under a vacuum overnight prior to hydration, vortexing, and spreading on a quartz slide. After equilibration overnight at room temperature, the sample was placed in a sealed wheel containing a saturated solution of K₂SO₄ to maintain the relative humidity at 93%. After 2 h of equilibration in the wheel, CD spectra were recorded on a Jasco J-815 spectrometer (Jasco Analytical Instruments, Easton, MD) at eight different angles (every 45°). The spectra were recorded at 298 K over a wavelength range of 190-260 nm using a scan speed of 100 nm/min, a 1 nm bandwidth, and four scans. To avoid artifacts from linear dichroism, samples were made by spreading over an area measuring approximately 10-12 mm in diameter and the signal was averaged over the eight measurements.⁴⁰ A blank containing lipids but no peptide was obtained and subtracted from the peptide signal to correct for the lipid background signal.

Preparation of Samples for Solid-State NMR. Oriented Samples. Oriented samples were prepared to quantify the order parameter of the lipid acyl chains in ²H solid-state NMR experiments. The samples were prepared according to a procedure that we previously described.³⁷ Briefly, aligned lipid bilayer preparations were made using 1:1 POPE/POPGd31 (Avanti Polar Lipids) to mimic bacterial cell membranes. The peptide and lipids were mixed in a mixture of chloroform and TFE to reach a peptide-to-lipid ratio of 1:60. Higher peptide concentrations were attempted but resulted in a significant powder pattern due to the disruption induced by the peptide, and therefore could not be reliably used to obtain quadrupolar splittings. Hydration of the peptide-lipid films was accomplished using 3 mM phosphate buffer at pH 6.0. After overnight binding, the samples were centrifuged and the pellet was spread on thin glass slides (dimensions $5.7 \times 12 \times 0.03$ mm³ from Matsunami Trading Co., Japan). The samples were equilibrated in a chamber maintained at a relative humidity higher than 90% using a saturated K2SO4 solution. Additional buffer at a ratio of 1 µL buffer for every 1 mg of peptide/lipid mixture was added. After being stacked, the slides were placed in a glass cell (Vitrocom Inc., NJ), sealed with beeswax, and incubated at 37 °C until the samples became homogeneously hydrated.

Peptide—DNA Samples. Samples were made by adding the peptide to a solution of duplex DNA (AAATACACTTTT-GGT) to condense the DNA into DNA-peptide aggregates that could be collected for solid-state NMR experiments. On the basis of the CD-monitored titrations, a 1:1 peptide-to-DNA molar ratio was used to work under conditions where enough condensed DNA-peptide could be harvested and the concentration of free peptide was negligible, and therefore did not interfere with the NMR experiments on the DNAbound peptide. The amount of piscidin averaged about 2-3 mg per sample. The samples were centrifuged (<2000 rpm) to remove excess hydration while maintaining the ratio of 69 water molecules per nucleotide needed to stabilize the B-form of DNA.41 Sample weight was recorded to ensure sufficient hydration.

Solid-State NMR Experiments. ²H Solid-State NMR. ²H solid-state NMR spectra were acquired at 305 K, above the phase transition temperature of the lipids, on a 400 MHz NMR spectrometer with a Bruker DRX console and quadrupolar echo pulse sequence. A low electrical field probe built at the National High Magnetic Field Laboratory (NHMFL) with a 90° pulse width of 3.05 μ s and an echo time of 30.0 μ s was used. Spectra

were processed with a line broadening of 50 Hz. ²H, a spin 1 nucleus, gives rise to quadrupolar splittings ($\Delta \nu_{O}$) that have a magnitude related to $S_{\rm CD}$, the order parameter of the corresponding CD bond.⁴² For oriented samples studied such that the bilayer normal is parallel to the static magnetic field, as was the case in this study, the expression for $\Delta \nu_{O}$ and S_{CD} is

$$\Delta \nu_{\rm Q} = \frac{3}{2} \chi S_{\rm CD} \tag{1}$$

where χ is the quadrupolar splitting constant (168 kHz for paraffin chains). ⁴² Qualitatively, a decrease in the quadrupole splitting of the signal from a deuterium nucleus indicates lower order of the acyl chain. In this study, the ²H quadrupolar splittings $\Delta
u_{Q}$ for the deuterons of the labeled palmitoyl chain were assigned as previously described. 42 To report the effect of each peptide, we compared the order parameter for each bond in a pure lipid "blank" sample ("S_{CD}(lipid)") against that in a peptide-containing sample ("S_{CD}(lipid + peptide)") to yield the absolute change in order parameter, $\Delta S_{\rm CD}$, and the normalized change in order parameter, $\Delta S_{\text{CD}}^{\text{norm}}$, as follows

$$\Delta S_{\rm CD} = S_{\rm CD}({\rm lipid}) - S_{\rm CD}({\rm lipid + peptide})$$
 (2)

$$\Delta S_{\rm CD}^{\rm norm} = \frac{\Delta S_{\rm CD}}{S_{\rm CD}({\rm lipid})} \tag{3}$$

¹⁵N/¹³C Distance Measurements. The REDOR measurements were carried out on a midbore 800 MHz magnet equipped with a Bruker Avance III console using an NHMFL 3.2 mm low-E triple-resonance biosolids MAS probe. The Larmor frequencies of ¹H, ¹³C, and ¹⁵N were 800.12, 201.19, and 81.08 MHz, respectively. The hydrated samples were transferred into a 3.2 mm thin-wall MAS rotor (36 uL sample volume) and sealed with tightly fitted caps to prevent loss of hydration during the NMR experiments. The sample spinning rate was controlled by a Bruker pneumatic MAS unit at 13 kHz ± 3 Hz. Details of the parameters used to set up the REDOR pulse sequence are given in the Supporting Information. During the REDOR experiments, the sample temperature was controlled to 280 \pm 0.1 K by a Bruker BVT-3000 unit, which was calibrated in separate experiments using 207Pb NMR of dilute lead nitrate (mixed with KBr at a mass ratio of 1:1). The ¹³C chemical shift was referenced to the carbonyl carbon resonance of glycine at 178.4 ppm relative to trimethylsilane (TMS).4

For each dephasing time (i.e., a multiple of rotor periods), two sets of data without and with the train of ¹⁵N 180° pulses were recorded, corresponding to the $^{13}\mathrm{C}$ signals without (S_0) and with (S) $^{15}\mathrm{N}$ dephasing. The number of scans used to accumulate the signals ranged from 10 240 to 30 720 depending on the dephasing time. Their difference ΔS over S_0 depends exclusively on the ${}^{13}\mathrm{C} - {}^{15}\mathrm{N}$ dipolar coupling, and a MATLAB program was used to fit the ratio of $\Delta S/S_0$ as a function of the dephasing time, thus yielding the internuclear distance between the ¹³C and ¹⁵N labeled sites. Further details about fitting the data and obtaining error bars are given in the Supporting Information.

■ RESULTS AND DISCUSSION

Antimicrobial Assays. On the basis of prior studies, p1 and p3 are more active on Gram-positive than Gram-negative bacteria, and p1 is more potent than p3. Here, we tested p1 and p3 on Gram-positive Bacillus megaterium, whose large size facilitated optimal conditions for confocal microscopy imaging, and on a Gram-negative *E. coli* strain not tested previously. As shown in Table 1, the MICs obtained on *E. coli* confirm that p1

Table 1. Antibacterial Activity of p1 and p3

		MIC (μM)	
bacteria	ATCC #a	P1	Р3
Bacillus megaterium	14581	2-10	2-10
Escherichia coli	14948	2-10	10-20

^aATCC #: American Type Culture Collection number.

is more active than p3 and agree with those previously obtained by Chekmenev et al.²⁵ on another *E. coli* strain (ATCC # 25922). The observation that p1 and p3 had similar MICs on *B. megaterium* is consistent with the trend that the two isoforms are similarly active against Gram-positive bacteria.¹⁵

At Sub-Lethal Concentrations, Both P1 and P3 Translocate across Bacterial Membranes and Access Intracellular Constituents. Confocal microscopy was performed using FITC-labeled p1 and p3. When piscidin was previously derivatized with fluorescein, it was reported to maintain the same antimicrobial potency.²⁹ Images of fixed E. coli and B. megaterium cells that had been incubated with sub-MIC (0.75 μ M) dose treatments of FITC-p1 and FITC-p3 for 30 min reveal that both isoforms cross the bacterial membranes and localize intracellularly (Figure 2). Since DAPI binds DNA, it can be used to demonstrate protein-nucleic acid colocalization in bacteria, and we utilized it to locate cellular areas rich in nucleic acids (aka "nucleoids") relative to the location of FITC-p1 and FITC-p3. As shown in Figure 2, E. coli and B. megaterium cells that were first treated with piscidin and then DAPI prior to washing and fixing uptook DAPI. For the large B. megaterium cells, normalized FITC- and DAPIfluorescence intensities correlate well over the long axis of each cell (Figure 2C). This observation is consistent with the colocalization of intracellular p1 and p3 to the nucleoids of Gram-positive bacteria. For the smaller E. coli cells, the nucleoid regions could not be resolved by confocal microscopy (Figure 2B and D); however, the imaged piscidin-treated E. coli cells displayed intracellular FITC fluorescence. We note that, on the basis of the confocal microscopy images of Kim et al.,²⁹ a peptoid analogue of piscidin 1-but not wild-type p1translocated E. coli after a markedly higher 3.4 µM dose treatment. However, the apparent discrepancy may come from using different imaging conditions and/or E. coli strains. Interestingly, the images with B. megaterium indicate that piscidin is concentrated at the septa, a phenomenon that has been reported for other AMPs^{44,45} and will be discussed further below.

Permeabilization of Bacterial Cell Membranes Occurs in a Dose-Dependent Fashion at Sub-Lethal Concentrations of P1 and P3 and Is More Pronounced with P1. To determine if piscidin's mode of cell entry at sublethal concentrations may be concomitant with permeabilization, we exposed the bacterial strain $E.\ coli\ ML35$ to p1 and p3 below their MICs (2–10 μ M as determined using the standard protocol applicable to the data in Table 1) and performed the β -galactosidase permeabilization assay. More precisely, the ability of p1 and p3 to permeate bacterial membranes was quantified on the basis of how much cleavage of ONPG into ONP occurred when the peptides altered the IM of $E.\ coli$ and released the ONPG-cleaving β -galactosidase enzyme from the

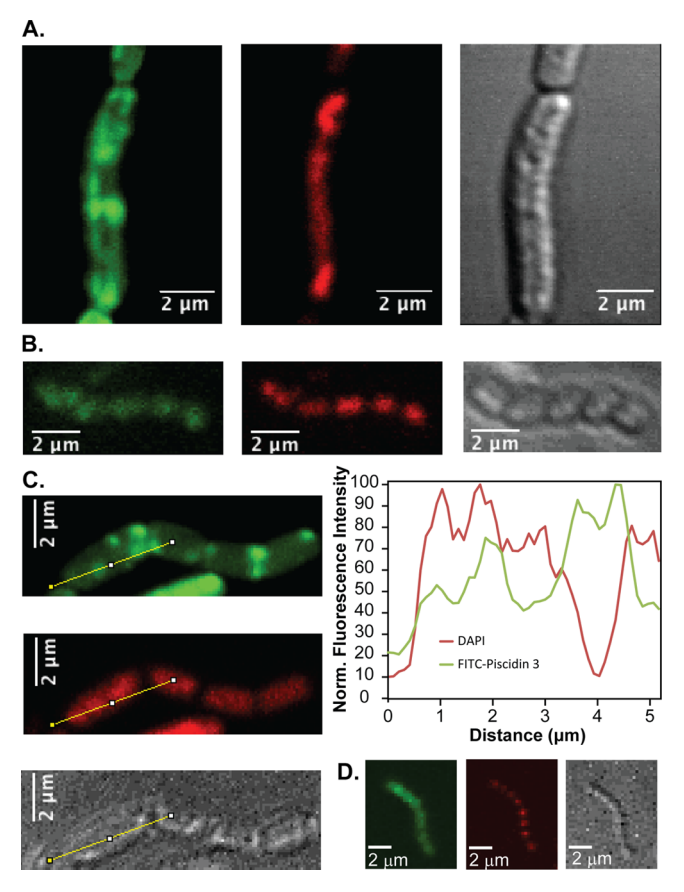


Figure 2. Co-localization between piscidins and the nucleoid regions of Gram-positive and Gram-negative bacteria. Confocal images of *B. megaterium* (A, C) and *E. coli* (B, D) treated first with 0.75 μ M FITC-p1 (A, B) or FITC-p3 (C, D) (green) followed by 0.75 μ M DAPI (red DNA marker) for another 30 min before washing with PBS. (D) Normalized fluorescence along the yellow line drawn across septating cells; the extremities and center of the lines are marked with squares. A high concentration of FITC-p3 is present at the septum appearing at a distance of 4 μ m along this line, while the DAPI signal is absent at this cellular location. Similar results were obtained with FITC-p1 and *B. megaterium*.

cytoplasm. ³⁸ As shown in Figure 3, beyond a threshold concentration of 0.25 μ M for p1 and 0.75 μ M for p3, permeabilization took place in a dose-dependent fashion and induced leakage that was more pronounced for p1 than p3. Notably, the leakage effectiveness of p1 leveled off at 0.75 μ M while that of p3 increased gradually throughout the tested range. At the end of the range, it took 4 times as much p3 (2 μ M) to reach the same leakage effectiveness as with p1 (0.5 μ M).

These results agree with prior findings that permeabilization of bacterial cell membranes can occur prior to lysis and cell death, and that coupling exists between peptide translocation and membrane leakage. Indeed, other AMPs also induce permeation below their MIC. For instance, temporin L also permeates cells in two steps that indicate a delineation between permeation and cell death: at low concentrations, it enters cells that become permeant to small molecules but remain alive; it is only at higher concentrations that larger intracellular compounds leak out and cell death occurs.

In terms of the site of membrane attack, piscidin may be opportunistic, since the log-phase *B. megaterium* cells treated with FITC-p3 revealed colocalization with the nascent septum

The Journal of Physical Chemistry B

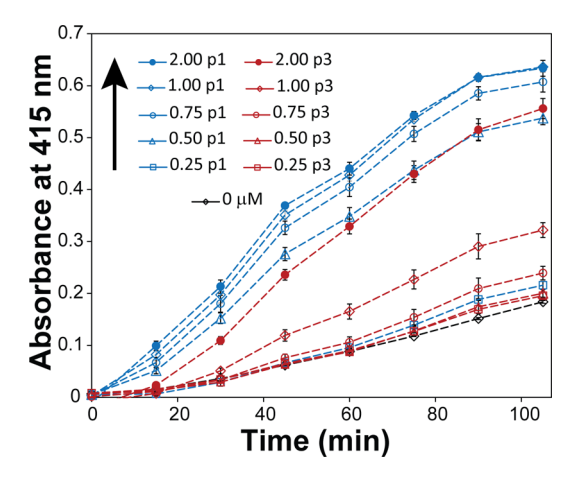


Figure 3. Permeabilization assays at sublethal concentrations of p1 and p3. ML-35 *E. coli* cells were incubated with p1 and p3 to characterize their ability to permeate bacterial membranes. The absorbance data at 415 nm for ONP are plotted for p1 (blue) and p3 (red) from bottom to top at 0 (black), 0.25, 0.50, 0.75, 1.0, and 2 μ M peptide concentrations (the 0.25 and 0.50 μ M data overlap for p3). The averages of triplicates are displayed along with the standard error.

(Figure 2C). LL-37 also selectively targets the structurally weaker septum membrane of some dividing bacteria such as *E. coli.* ^{44,45} Indeed, the real-time activity of LL-37 on *E. coli* cells revealed two stages when the peptide concentration was 8 μ M (4 times the MIC). Initially, the peptide accumulated on the cell membrane, probably interacting with the anionic lipopolysaccharides (LPS) in the outer membrane (OM). Translocation in septating cells allowed the peptide to enter and spread into the periplasm. At that point, growth was inhibited, possibly due to disruption of the cell envelope. Cells being complex systems, we moved on to quantifying the effects of p1 and p3 on isolated DNA and model membranes.

Calcein Release from 1:1 POPE/POPG Large Unilamellar Vesicles Is More Pronounced with P1 Than P3. To specifically characterize the membrane permeabilization effects of p1 and p3, release of calcein from LUVs constituted of 1:1 POPE/POPG that mimic *E. coli* bacterial cell membranes was monitored by fluorimetry at pH 7.4. In Figure 4, we report

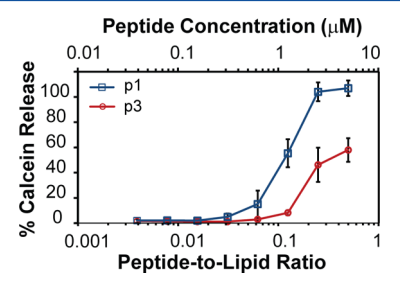


Figure 4. Percent release of calcein from LUVs made of 1:1 POPE/POPG after 3 min of exposure to increasing amounts of p1 and p3 at pH 7.4.

the percentage of leakage from the LUVs as a function of peptide-to-lipid ratio (P/L) and peptide concentration. Both peptides caused leakage from the LUVs, but p1 was significantly more permeabilizing than p3, giving rise to respective EC₅₀ values (effective concentration of peptide yielding 50% leakage) of 1.1 (P/L = 1:10) and 3.5 (P/L = 1:3) μ M. Notably, this effectiveness of p1 is stronger than that of p3 by a magnitude

 (~ 4) that is on par with that observed in the aforementioned permeabilization assays on E. coli. Overall, these dye leakage results track closely with the trend exhibited in the permeabilization (namely, that p1 is more active than p3 by a factor of ~4) and antimicrobial assays, and therefore validate the use of 1:1 POPE/POPG as a bacterial membrane model that reflects the stronger membrane activity of p1 as well as its more potent antimicrobial effects assuming that membrane disruption is the major factor contributing to its biological activity. The higher hydrophobicity of p1 compared to p3 combined with its imperfect amphipathicity (Figure 1) may explain its stronger membrane activity by allowing more pronounced perturbation of the lipid packing and mixing of the polar and nonpolar regions of the bilayer. 9,46-48 Interestingly, the onset of dye leakage just below 1 μ M and a P/L of 1:16 for p1 agrees well with the values obtained for the start of the bactericidal activity of PMAP-23, a 23-meric AMP that was studied on live E. coli cells to precisely characterize the critical P/L ratio for cell death and demonstrate that lipid vesicles are reliable systems to study the interactions of AMPs with cell membranes. 49 They can also be used to study the permeabilization capability of peptides in a competitive lipid bilayer environment.⁵⁰ As explained by the authors of the PMAP-23 study, the high P/L required to achieve cell death is consistent with a carpet mechanism, where membrane permeabilization results from peptide accumulation on the cell surface. In the case of piscidin, the leakage at high P/L corroborates the carpet mechanism previously postulated on the basis of solid-state NMR data.^{26,2}

Lipid Acyl Chain Order Parameters Indicate Interfacial Incorporation of P1 and P3 into 1:1 POPE/POPG Model Membranes. Increased disorder in phospholipid bilayers exposed to AMPs is a phenomenon known to accompany membrane thinning and increased trans-gauche isomerization of the acyl chains when peptides bind interfacially. Measuring the quadrupolar splittings of deuterons in methylene and terminal methyl groups of deuterated acyl chains by ²H solidstate NMR is particularly well suited to quantifying the disorder. 51 Here, the effects of p1 and p3 on bacterial cell mimics made of 1:1 POPE/POPG-d31 (i.e., with the palmitoyl chain of POPG as the deuterium reporter) were characterized in wide-line ²H NMR spectra obtained in the absence and presence of p1 and p3 at a P/L of 1:60 (Figure 5). At higher P/ L, distortions of the baseline due to the underlying powder pattern, probably induced by major disruptive effects of piscidin, prevented accurate determination of accurate quadrupolar splittings; thus, the data are interpreted at a P/L of 1:60. Two major findings emerge from these spectra. First, the percent decrease in the quadrupolar splittings (Table S1) demonstrates the membrane disordering effect of piscidin on the lipid acyl chain order, and hence the bilayer's susceptibility to the peptide. More specifically, the percent decrease in quadrupolar splittings of the methyl group is greater than that of the plateau region (formed by C2-C7 of the acyl chain), which is consistent with the "basket effect", where the binding of piscidin close to the headgroups of the phospholipid bilayers forces the rearrangement of the lipid tails to fill gaps under the surface-bound peptide. 52,53 Second, the results suggest that p1 has stronger disordering effects than p3 within the margin of error (± 0.25 kHz). Overall, these experiments show that both p1 and p3 are interfacially incorporated into the POPE/POPG bilayers and induce disorder in the bilayer even at a P/L of

The Journal of Physical Chemistry B

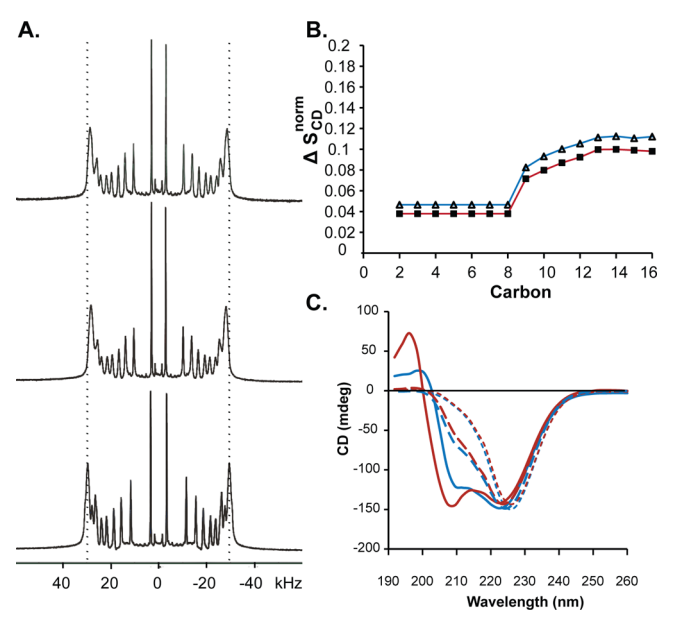


Figure 5. Acyl chain order parameters and orientations of p1 and p3 measured in 1:1 POPE/POPG membranes. (A) ²H NMR spectra for 1:1 POPE/POPG-d31 model membranes in the absence (bottom) and presence of p1 (middle) and p3 (top). The data were recorded on a 400 MHz spectrometer at 305 K and a frequency of 61.4 MHz. (B) Normalized changes in order parameters of the palmitoyl chain of the anionic lipid POPG-d31 upon addition of p1 (blue) and p3 (red) to 1:1 POPE/POPG-d31. (C) Oriented circular dichroism of p1 (blue) and p3 (red) at P/L values of 1:150 (solid line), 1:40 (long dashes), and 1:25 (short dashes) in 1:1 POPE/POPG at 298 K.

1:60, which is below the threshold leading to leakage in the calcein release experiments.

Notably, the order parameters of C-D bonds in the palmitoyl chain are higher in POPE- than 1-palmitoyl-2oleoyl-sn-glycero-3-phosphatidylcholine (POPC)-containing bilayers.⁵⁴ This has been attributed to the smaller area per molecule of membranes containing PE headgroups (which are smaller than PC in size) as known from X-ray diffraction data. 55 Given the higher order of POPE-containing membranes and the resulting higher surface density, one might expect the membrane to become more resistant to the action of piscidins because ordered membranes are generally known to be less permeable.⁵⁶ However, this did not prevent p1 and p3 from decreasing the order of the acyl chains throughout the PG chains in mixed PE/PG. The results could have important ramifications, since bilayer fluidity and composition are aspects that bacteria modify as part of their mechanisms of drug resistance, but p1 and p3 have membrane disordering effects even when membranes contain 50% POPE. Interestingly, pleurocidin, a member of the piscidin family, is also able to disrupt bilayers containing a high amount of PE.57

Both P1 and P3 Adopt Tilted/Transmembrane Orientations When Their Concentration Is Increased in 1:1 POPE/POPG Model Membranes. Since piscidin translocates across membranes, permeabilizes *E. coli* membranes and induces strong dye leakage in model membranes, we used OCD to determine if the peptide could adopt an orientation conducive to translocation and leakage when it interacts with membranes. Figure 5C shows the OCD data for p1 and p3 in 1:1 POPE/POPG at pH 7.4. At 1:150 P/L, the signal has the features expected for the surface-bound state (S-state), namely, (almost) equal intensities at 208 and 222 nm. When a P/L of

1:40 is reached, decreased intensity of the shoulder at 208 nm indicates the disappearance of the S-state as it converts to a tilted state (T-state) or coexists with a transmembrane state that is parallel to the bilayer normal (TM-state). At a P/L of 1:25, the shoulder has almost completely vanished, indicating that the T- and/or TM-states predominate. We did not attempt to quantify the amount of each state and compare the respective abilities of p1 and p3 to tilt in the membrane due to the amount of scattering in the multilayered phospholipid bilayers used in these experiments.⁵⁸ Notwithstanding, these results show that p1 and p3 tilt into the membrane at high concentrations and tilting in a TM- or T-orientation may play a role in the activity of the peptides, since it occurs in the range of P/L ratios inducing the calcein leakage described above. However, we note that the threshold for the appearance of the tilted state (<1:40 for p1 and p3) is lower than that observed for the onset of permeabilization in the dye leakage assays (\sim 1:32 for p1 and 1:16 for p3). It is also true that the solidstate NMR data of the peptides at a 1:20 P/L ratio do not show a TM- or T-state.²⁶ Such disparities could be due to (1) T- or TM-states not forming pores or defects large enough to be leaky at the lowest P/L ratios; (2) lower hydration level in the OCD samples (11 water molecules per lipid)⁵⁹ stabilizing the tilted state (that would otherwise be short-lived and not captured by NMR done at a hydration of 50 waters per lipid)²⁶ because the lower hydration of the bilayer could heighten repulsion between peptide molecules bound in the S-state and force them to settle in the bilayer core in a T- or TM-state.

The mechanism by which charged peptides translocate across bacterial membranes is not fully understood. It is possible that peptides tilt in bacterial membranes and translocate by taking advantage of transient defects in the membrane and/or oxidized lipids that may form following exposure to the reactive oxygen species released during phagocytosis in the host. 32,60 On the basis of the interfacial activity model, nascent lipid defects could be stabilized by piscidin and/or disordered toroidal pores could form, allowing the peptide to reorient in the membrane to cross it without experiencing a long-lived TM- or T-state (unless lower hydration stabilizes it). This process would occur even at low (e.g., sublethal) peptide concentrations due to the driving force of equilibrating peptide concentrations on each side of the membrane. Structurally, kinks in the structures of AMPs may facilitate flipping in the membrane as an intermediate step to -64 Here, the ability of p1 and p3 to penetrate crossing it. bacterial membranes and localize intracellularly at concentrations below those that would be needed to fatally lyse the membrane may be related to the Gly13-mediated kink that has been recently identified by NMR structures of both p1 and p3.²⁶ Interestingly, the proline hinge of buforin II, a remarkably similar and helix-disrupting structural feature, may be implicated in its translocation capacity.⁶⁵

Both P1 and P3 Bind and Condense Isolated DNA, but P3 Is More Effective. Ability of P1 and P3 to Retard DNA Gel Migration. That p1 and p3 appear to colocalize with the nucleoids behooves the question that they may exhibit an intracellular mechanism of antibacterial action, which could, as in the case of its relative pleurocidin, involve interactions with nucleic acids. The gel retardation assay was employed to illuminate DNA binding *in vitro*. Both p1 and p3 were shown to bind isolated DNA; as the concentration of each isoform increased, more DNA was neutralized in terms of charge and/or became aggregated, and therefore was restricted from migrating through the gel (Figure 6). As shown by the fits in

The Journal of Physical Chemistry B

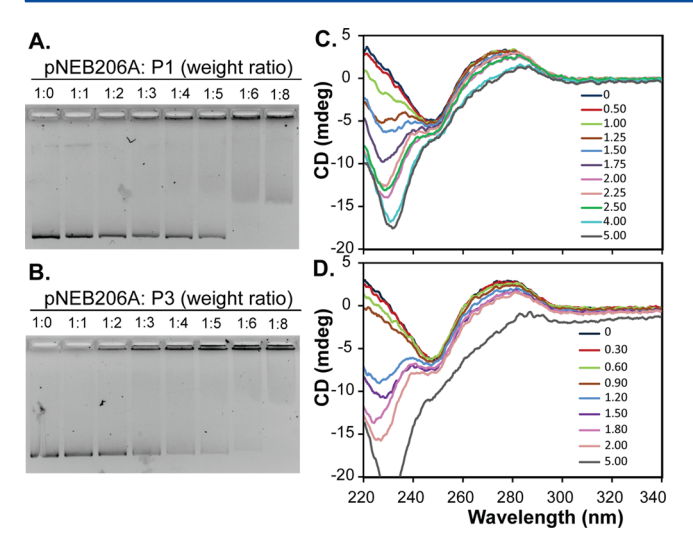


Figure 6. Binding of p1 and p3 to isolated DNA. (A, B) Gel retardation assay experiments on p1 (A) and p3 (B). Each well contained 100 ng of linearized plasmid DNA and increasing amounts of p1 or p3 at pH 7.4. The gel was soaked in ethidium bromide for visualization. (C, D) Circular dichroism titration experiments at 2.0 μ M DNA (AAATACACTTTTGGT) and increasing p1-DNA (C) or p3-DNA (D) molar ratios at pH 7.4.

Figure 7, the respective peptide-to-DNA weight ratio leading to 50 and 90% inhibition of DNA migration are 4.4 and 7.2 for p1,

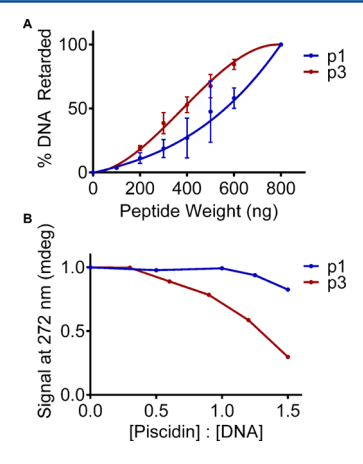


Figure 7. Analysis of p1 and p3 effects following binding to DNA. (A) Percent retardation of DNA as the peptide to DNA weight ratio increases and the linearized plasmid DNA is neutralized in terms of charge and/or becomes aggregated by the amphipathic peptide at pH 7.4. (B) Normalized values for the CD signal of DNA (AAATACACTTTTGGT) monitored at 272 nm as a function of peptide dose up to a 1.5:1 peptide-to-DNA molar ratio at pH 7.4.

while they are only 3.9 and 6.4 for p3, indicating that p3 retards DNA gel migration more readily than p1.

Ability of P1 and P3 to Condense DNA. In a previous study, a 15-base-pair DNA sequence bound to a section of histone H2A homologous to buforin II was used to study via CD-monitored titrations the DNA-interacting and -condensing ability of buforin II, magainin 2, and pleurocidin.³⁹ Similar to some salts and polymers, cationic AMPs can induce DNA aggregation into polymer-and-salt-induced (psi- or Ψ-) condensates that have been ascribed to compacted DNA, typically highly ordered superhelical structures.⁶⁶ Here, we also followed by CD the extent to which p1 and p3 bind and

compact DNA in vitro. The signature of B-DNA includes strong positive and negative CD signals in the 260-290 and 230-260 nm ranges, respectively. As cationic piscidin is added to anionic DNA, the CD signal between 260 and 290 nm collapses, reflecting peptide-induced, dose-dependent condensation of DNA (Figure 6C and D). The CD spectra contain the characteristic circular intensity differential light scattering known to reflect the presence of Ψ-condensates.³⁹ Since the drop in signal intensities at 272 nm provided a good representation of the DNA-binding affinity of buforin II, magainin 2, and pleurocidin,³⁹ we similarly plotted the values for piscidin-to-DNA titration ratios preceding excessive scattering, as estimated by UV monitoring of the samples (Figure 7B). According to these plots, p3 is more effective than p1 at retarding and condensing DNA. This distinction supplements gel retardation assay results well and leads to the conclusion that the peptide with the stronger DNAretarding ability is also the one that more effectively compacts DNA into highly ordered structures.

The comparatively enhanced ability of p3 to interact with DNA may be explained by its amino acid sequence. While p1 has two arginines, p3 contains an additional one at position 14 (Figure 1); notably, buforin II's strong affinity for DNA is likely driven by arginine-DNA interactions.⁶⁵ Moreover, Gly17 in p3, whose equivalent in p1 is an uncharged histidine at pH 7.4, may provide p3 with additional flexibility needed to bind and alter the conformation of duplex DNA. Since different sequences of DNA were used in the CD experiments and the gel retardation assay, it is likely that piscidins do not require a specific DNA sequence for binding. Indeed, if piscidin is similar to buforin II in terms of its mechanism of DNA binding being driven by interactions between its basic residues and the DNA phosphate groups, then p1 and p3 may similarly be expected to interact with DNA independent of its nucleic acid sequence. 65 In this regard, the gel data displayed in Figure 7A indicate that the plots for p1 and p3 converge at 100% DNA retardation; i.e., the same amount of p1 and p3 is needed to reach full retardation even though p3 gets there in a more hyperbolic fashion than p1. Precipitation of DNA by amphipathic peptides represents an interesting situation, since not only do the cationic peptides neutralize charges on the DNA (and thus lower its solubility), but they also present their cationic face to the DNA, thereby leaving the hydrophobic side exposed to the aqueous environment. Presumably, this unfavorable state translates into favorable aggregation of DNA-peptide complexes via the exposed nonpolar residues of the peptide, and therefore creates another path for decreased solubility. Precedents of similar DNA aggregation and involvement of hydrophobic chemical groups exist for synthetic materials such as mannobiose-modified polyethylenimines.⁶⁷ Here, since p1 is more hydrophobic than p3 (Figure 1), a cooperative effect that enhances compaction may take place once a threshold amount of p1 has bound DNA, and this could explain the seemingly sigmoidal behavior of p1's binding while that of p3 is more hyperbolic (Figure 7A).

Solid-State NMR Structural Studies Indicate That P1 and P3 Are α -Helical When Bound to DNA. While the above CD studies clearly document the binding of piscidin to DNA, they do not establish the structural features of piscidin in the bound state. A major issue with CD is that the peptide and DNA signals overlap in the region between 190 and 250 nm, which prevents the clear detection of signals important to decipher the secondary structure of the peptide. The problem is

further exacerbated by the precipitation of the peptide–DNA complexes. Fortuitously, solid-state NMR is a powerful technique to study aggregated complexes. Here, we used rotational-echo double-resonance (REDOR) NMR⁶⁸ within ¹⁵N- and ¹³C-labeled p1 and p3 peptides to determine their secondary structures in the Ψ-condensates. We hypothesized that the amphipathic nature of piscidin folded into an α-helix would create favorable interactions with DNA and therefore favor binding to it. The ¹³C-carbonyl and ¹⁵N-amide labels were placed at positions *i* and *i* + 4 to span the distance of a hydrogen bond (~4.2 Å) in the hypothesized α-helix, while this $^{13}C_i/^{15}N_{i+4}$ distance in a β-sheet or extended structure is too long (>5 Å) to be measurable by REDOR.³⁷ As shown in Figure 8, the 4.30 ± 0.55 Å distance in $^{13}C-G_8/^{15}NV_{12}$ p1 and

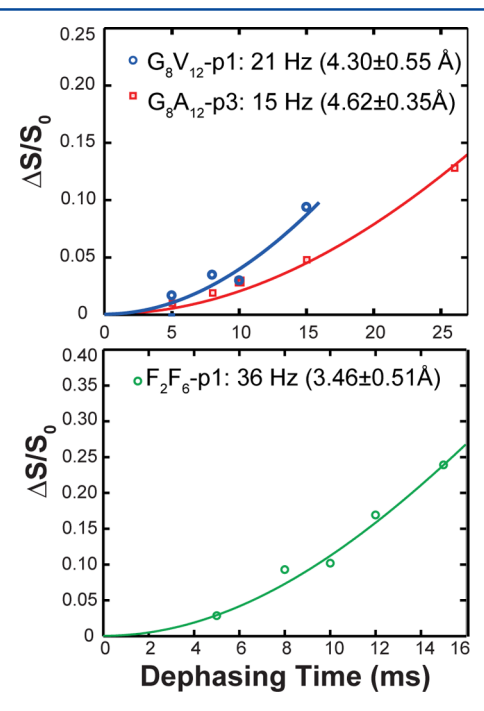


Figure 8. Secondary structure of p1 and p3 bound to DNA. REDOR solid-state NMR 13 C/ 15 N distance measurements between the 13 C of the carbonyl at position i and the 15 N of the amide at position i + 4 in p1 (blue and green) and p3 (red). The measured distances on the order of 4 Å are consistent with α -helicity. Hydrated samples prepared at pH 7.4 were investigated by NMR at 280 K on a 800 MHz spectrometer. Representative spectra are shown in Figure \$1.

 4.62 ± 0.35 Å in $^{13}\text{C-G}_8/^{15}\text{N-A}_{12}$ p3 confirm lpha-helicity, whereas the shorter distance of 3.46 \pm 0.51 Å in ${}^{13}\text{C-F}_2/{}^{15}\text{N-F}_6$ p1 indicates a tighter structural arrangement at the N-end but more structural restraints are needed to characterize it at high resolution. Interestingly, p3 gave rise to sharper signals than p1, which would be consistent with increased motional averaging in p3, and therefore a reduced ¹³C/¹⁵N dipolar coupling and increased ¹³CG₈-¹⁵N-A₁₂ distance. Alternatively, the sharper lines may indicate that p3 adopts a structure that is more homogeneous than that of p1, possibly because the arginine at position 14 in p3 interacts more strongly with DNA than the lysine at the same position in p1. The details of the helical structure of piscidin bound to DNA are not known, but they are expected to differ from those obtained in 1:1 POPE/POPG, since the initial electrostatic attraction of peptides to anionic membranes is followed by an insertion that is driven by hydrophobic interactions. In contrast, binding to DNA buries

the hydrophilic side chains, leaving the hydrophobic ones exposed to the solvent. Binding to the relatively rigid surface of DNA would require adjustment of the peptide's structure in a way that is different from optimizing contacts with hydrophobic bilayers but achievable thanks to the plasticity of the α -helix and flexibility of numerous glycine and serine residues. ⁶⁹

CONCLUSIONS

AMPs are crucial molecules that provide a first line of defense in the fight against pathogens. Endowed with flexible amphipathic structures, they are inherently able to recognize and interact with a broad range of pathogens and cellular components. As mentioned in the Introduction, it is not a straightforward task to establish the relative contributions of various mechanisms of action to the lethality of AMPs. 12 Here, our results on p1 and p3, both of which are good archetypes of AMPs, span three major facets that taken together allow us to compare the relative abilities of these two natural peptides to affect biological membranes and DNA. First, p1 and p3 (Figure 1), which are known to interact and disrupt lipid bilayers, are demonstrated to translocate across bacterial membranes at sublethal concentrations (Figure 2), and this is accompanied by permeation in E. coli that leads to more significant leakage with p1 (Figure 3). In model membranes, p1 is also more membrane-active than p3 (Figures 4 and 5). Since permeation occurs below the MIC, it is not necessarily the step inducing cell death, in agreement with observations on other AMPs and the idea that pores and/or defects may not be lethal until they reach a certain threshold size. Second, inside the cells, both p1 and p3 are colocalized with nucleoids (Figure 2). Third, in vitro, both peptides bind DNA in an α -helical conformation (Figure 8) and structurally disrupt it, but p3 is more effective at retarding and condensing DNA into highly ordered structures (Figures 6 and 7). These findings, which lay the groundwork for further investigations to determine the significance of piscidin's ability to access the cytoplasm at sublethal concentration and bind DNA, provide a backdrop for several concluding points, as follows. First, we find that, as previously postulated, the ability to translocate and access intracellular targets appears to be found in specific families of AMPs, since several members of the piscidin family, including pleurocidins, 36 have now been shown to translocate, but not all AMPs have demonstrated this property. Second, at sublethal concentrations, both p1 and p3 permeabilize E. coli membranes (Figure 2) and p1 is more effective in the ML35 cells; therefore, both peptides have an opportunity for cell penetration and intracellular accumulation to an extent that very likely varies depending on the peptide and its bacterial targets. Higher MICs on Gram-negative bacteria may be due to diversion of some peptide in the periplasm of these bacteria via the septum (Figure 2), an effect that would be absent in the Gram-positive bacteria and would leave more peptide to act on targets such as the membrane and nucleic acids. Third, whether enough peptide can translocate and accumulate into the cytoplasm to affect DNA is uncertain, but within the nucleoids, a mechanism of action for piscidin that complements its membrane activity could include affecting processes such as protein synthesis, as was discovered for Bac₁₋₃₅. ¹³ Fourth, piscidin is found to accumulate at the septum where the membrane is weaker (Figure 2). Interestingly, CRAMP (16-33) inhibits the FtsZ assembly that forms at the midcell position where the septum will then appear; 70 this mechanism may be applicable to piscidin. Fifth, the relative abilities of the two piscidin isoforms

to condense DNA do not correlate with their respective antibacterial potency: although p1 is typically a more potent AMP than p3 on Gram-negative bacteria (Table 1), 15,25 the latter isoform compacts DNA more readily than does the former (Figures 6 and 7). Since p1 is more membrane disruptive than p3, it is tempting to infer that the bactericidal activity is mostly governed by piscidin's membranolytic effects as a primary mechanism of action, once enough peptide has accumulated on the bacterial membrane. However, since p1 and p3 have similar MICs on a significant number of bacteria (e.g., Gram-positive), it is possible that p3 relies on a supplementary mechanism of action on these bacteria to compensate for weaker membranolytic effects. In fact, the ability to translocate across the membrane of Gram-positive bacteria (that do not have a periplasm) and affect DNA (or other intracellular targets) more effectively than p1 could explain how p3 makes up for lower membrane activity than p1, and thereby remains generally as effective as p1 on these bacteria. Sixth, the finding that the two homologues have complementary effects on DNA and lipid membranes raises an interesting question with regard to the recognized synergy that exists between the AMPs expressed by a given organism.⁶ Complementary effects within the piscidin family may help members act more broadly on pathogens. In fact, it may be a critical aspect of minimizing bacterial resistance and could be an important feature to incorporate in the design of novel drugs to combat drug-resistant bacteria. From this perspective, optimizing a peptide to be the strongest of its family on all targets (e.g., membranes, DNA) may not be beneficial to the organism because the higher incidence of bacterial resistance that it could induce would lead to an evolutionary dead-end, which is seemingly circumventable by a group of peptides with complementary effects. Ultimately, understanding the biological significance and specific physicochemical details of membrane translocation and nucleic acid binding ability by members of the piscidin family will not only help further understand their multifunctionality and polyreactivity but also establish the knowledge needed to design novel therapeutic drugs with improved specificity, synergy, and potency.

ASSOCIATED CONTENT

S Supporting Information

The Supporting Information is available free of charge on the ACS Publications website at DOI: 10.1021/acs.jpcb.5b09685.

Table and details regarding the analysis of the REDOR and ²H solid-state NMR data as well as additional information about sample preparation and complete author list for references with more than 10 authors (PDF)

AUTHOR INFORMATION

Corresponding Author

*Phone: (315) 859-4243. Fax: (315) 859-4807. E-mail: mcotten@hamilton.edu.

Notes

The authors declare no competing financial interest.

ACKNOWLEDGMENTS

This research was supported by a National Science Foundation CAREER grant (CHE-0832571) to M.L.C., a Henry Teacher-Scholar Award from the Henry and Dreyfus Foundation to M.L.C., and the Hamilton College Departments of Biology and

Chemistry. The authors would also like to acknowledge Dr. Wei-Jen Chang, Ken Bart, and Nikolaus Wagner from Hamilton College and Dr. Paul J. Linser from the University of Florida. The authors are also thankful to Dr. André J. Ouellette from the University of Southern California for his generous gift of the *E. coli* ML-35 strain used in the permeabilization assays. The solid-state NMR experiments were carried out at the National High Magnetic Field Lab (NHMFL) supported by the NSF Cooperative agreement DMR-1157490 and the State of Florida.

ABBREVIATIONS

AMP, antimicrobial peptide; *B. megaterium, Bacillus megaterium*; DAPI, 4′,6-diamidino-2-phenylindole; *E. coli, Escherichia coli*; FITC, fluorescein isothiocyanate; HDP, host defense peptide; IM, inner membrane; OCD, oriented circular dichroism; OM, outer membrane; ONPG, ortho-nitrophenyl-β-galactoside; ONP, *o*-nitrophenol; p1, piscidin 1; p3, piscidin 3; POPC, 1-palmitoyl-2-oleoyl-*sn*-glycero-3-phosphatidylcholine; POPE, 1-palmitoyl-2-oleoyl-*sn*-glycero-3-phosphatidylethanolamine; POPG, palmitoyl-2-oleoyl-*sn*-glycero-3-phosphoglycerol; P/L, peptide-to-lipid ratio; psi-condensates, polymer-and-salt-induced condensates; REDOR, rotational-echo double-resonance

REFERENCES

- (1) Zasloff, M. Antimicrobial Peptides of Multicellular Organisms. *Nature* **2002**, *415*, 389–395.
- (2) Fjell, C. D.; Hiss, J. A.; Hancock, R. E. W.; Schneider, G. Designing Antimicrobial Peptides: Form Follows Function. *Nat. Rev. Drug Discovery* **2011**, *11*, 37–51.
- (3) Boman, H. G. Antibacterial Peptides: Basic Facts and Emerging Concepts. J. Intern. Med. 2003, 254, 197–215.
- (4) Shai, Y. Mode of Action of Membrane Active Antimicrobial Peptides. *Biopolymers* **2002**, *66*, 236–248.
- (S) Hilchie, A. L.; Wuerth, K.; Hancock, R. E. Immune Modulation by Multifaceted Cationic Host Defense (Antimicrobial) Peptides. *Nat. Chem. Biol.* **2013**, *9*, 761–768.
- (6) Bahar, A. A.; Ren, D. Antimicrobial Peptides. *Pharmaceuticals* **2013**, *6*, 1543–1575.
- (7) Marcellini, L.; Borro, M.; Gentile, G.; Rinaldi, A. C.; Stella, L.; Aimola, P.; Barra, D.; Mangoni, M. L. Esculentin-1b(1–18)–a Membrane-Active Antimicrobial Peptide That Synergizes with Antibiotics and Modifies the Expression Level of a Limited Number of Proteins in Escherichia Coli. *FEBS J.* **2009**, *276*, 5647–5664.
- (8) Fox, J. L. Antimicrobial Peptides Stage a Comeback. *Nat. Biotechnol.* **2013**, 31, 379–382.
- (9) Wimley, W. C. Describing the Mechanism of Antimicrobial Peptide Action with the Interfacial Activity Model. *ACS Chem. Biol.* **2010**, *5*, 905–917.
- (10) Henriques, S. T.; Melo, M. N.; Castanho, M. A. Cell-Penetrating Peptides and Antimicrobial Peptides: How Different Are They? *Biochem. J.* **2006**, 399, 1–7.
- (11) Yount, N.; Yeaman, M. Immunocontinuum: Perspectives in Antimicrobial Peptide Mechanisms of Action and Resistance. *Protein Pept. Lett.* **2005**, *12*, 49–67.
- (12) Nicolas, P. Multifunctional Host Defense Peptides: Intracellular-Targeting Antimicrobial Peptides. FEBS J. 2009, 276, 6483–6496.
- (13) Mardirossian, M.; Grzela, R.; Giglione, C.; Meinnel, T.; Gennaro, R.; Mergaert, P.; Scocchi, M. The Host Antimicrobial Peptide Bac71–35 Binds to Bacterial Ribosomal Proteins and Inhibits Protein Synthesis. *Chem. Biol.* **2014**, *21*, 1639–1647.
- (14) Lauth, X.; Shike, H.; Burns, J. C.; Westerman, M. E.; Ostland, V. E.; Carlberg, J. M.; Van Olst, J. C.; Nizet, V.; Taylor, S. W.; Shimizu, C.; et al. Discovery and Characterization of Two Isoforms of Moronecidin, a Novel Antimicrobial Peptide from Hybrid Striped Bass. *J. Biol. Chem.* **2002**, *277*, 5030–5039.

- (15) Silphaduang, U.; Noga, E. J. Peptide Antibiotics in Mast Cells of Fish. *Nature* **2001**, 414, 268–269.
- (16) Silphaduang, U.; Colorni, A.; Noga, E. J. Evidence for Widespread Distribution of Piscidin Antimicrobial Peptides in Teleost Fish. *Dis. Aquat. Org.* **2006**, *72*, 241–252.
- (17) Baccari, G. C.; Pinelli, C.; Santillo, A.; Minucci, S.; Rastogi, R. K. Mast Cells in Nonmammalian Vertebrates: An Overview. *Int. Rev. Cell Mol. Biol.* **2011**, 290, 1–53.
- (18) Chinchar, V. G.; Bryan, L.; Silphaduang, U.; Noga, E.; Wade, D.; Rollins-Smith, L. Inactivation of Viruses Infecting Ectothermic Animals by Amphibian and Piscine Antimicrobial Peptides. *Virology* **2004**, 323, 268–275.
- (19) Wang, G. Database-Guided Discovery of Potent Peptides to Combat Hiv-1 or Superbugs. *Pharmaceuticals* **2013**, *6*, 728–758.
- (20) Lin, H.-J.; Huang, T.-C.; Muthusamy, S.; Lee, J.-F.; Duann, Y.-F.; Lin, C.-H. Piscidin-1, an Antimicrobial Peptide from Fish (Hybrid Striped Bass Morone Saxatilis X M. Chrysops), Induces Apoptotic and Necrotic Activity in Ht1080 Cells. *Zool. Sci.* **2012**, *29*, 327–332.
- (21) Apponyi, M. A.; Pukala, T. L.; Brinkworth, C. S.; Maselli, V. M.; Bowie, J. H.; Tyler, M. J.; Booker, G. W.; Wallace, J. C.; Carver, J. A.; Separovic, F.; et al. Host-Defence Peptides of Australian Anurans: Structure, Mechanism of Action and Evolutionary Significance. *Peptides* **2004**, *25*, 1035–1054.
- (22) Lee, E.; Shin, A.; Jeong, K. W.; Jin, B.; Jnawali, H. N.; Shin, S.; Shin, S. Y.; Kim, Y. Role of Phenylalanine and Valine10 Residues in the Antimicrobial Activity and Cytotoxicity of Piscidin-1. *PLoS One* **2014**, *9*, e114453.
- (23) Huang, H. N.; Chan, Y. L.; Hui, C. F.; Wu, J. L.; Wu, C. J.; Chen, J. Y. Use of Tilapia Piscidin 3 (Tp3) to Protect against Mrsa Infection in Mice with Skin Injuries. *Oncotarget* **2015**, *6*, 12955–12969.
- (24) Chen, W. F.; Huang, S. Y.; Liao, C. Y.; Sung, C. S.; Chen, J. Y.; Wen, Z. H. The Use of the Antimicrobial Peptide Piscidin (Pcd)-1 as a Novel Anti-Nociceptive Agent. *Biomaterials* **2015**, *53*, 1–11.
- (25) Chekmenev, E. Y.; Vollmar, B. S.; Forseth, K. T.; Manion, M. N.; Jones, S. M.; Wagner, T. J.; Endicott, R. M.; Kyriss, B. P.; Homem, L. M.; Pate, M.; et al. Investigating Molecular Recognition and Biological Function at Interfaces Using Piscidins, Antimicrobial Peptides from Fish. *Biochim. Biophys. Acta, Biomembr.* **2006**, 1758, 1359—1372.
- (26) Perrin, B. S., Jr.; Tian, Y.; Fu, R.; Grant, C. V.; Chekmenev, E. Y.; Wieczorek, W. E.; Dao, A. E.; Hayden, R. M.; Burzynski, C. M.; Venable, R. M.; et al. High-Resolution Structures and Orientations of Antimicrobial Peptides Piscidin 1 and Piscidin 3 in Fluid Bilayers Reveal Tilting, Kinking, and Bilayer Immersion. *J. Am. Chem. Soc.* **2014**, *136*, 3491–3504.
- (27) De Angelis, A. A.; Grant, C. V.; Baxter, M. K.; McGavin, J. A.; Opella, S. J.; Cotten, M. L. Amphipathic Antimicrobial Piscidin in Magnetically Aligned Lipid Bilayers. *Biophys. J.* **2011**, *101*, 1086–1094.
- (28) Chekmenev, E.; Vollmar, B.; Cotten, M. Can Antimicrobial Peptides Scavenge around a Cell in Less Than a Second? *Biochim. Biophys. Acta, Biomembr.* **2010**, *1798*, 228–234.
- (29) Kim, J. K.; Lee, S. A.; Shin, S.; Lee, J. Y.; Jeong, K. W.; Nan, Y. H.; Park, Y. S.; Shin, S. Y.; Kim, Y. Structural Flexibility and the Positive Charges Are the Key Factors in Bacterial Cell Selectivity and Membrane Penetration of Peptoid-Substituted Analog of Piscidin 1. *Biochim. Biophys. Acta, Biomembr.* 2010, 1798, 1913–1925.
- (30) Jiang, Z.; Vasil, A. I.; Vasil, M. L.; Hodges, R. S. "Specificity Determinants" Improve Therapeutic Indices of Two Antimicrobial Peptides Piscidin 1 and Dermaseptin S4 against the Gram-Negative Pathogens Acinetobacter Baumannii and Pseudomonas Aeruginosa. *Pharmaceuticals* **2014**, *7*, 366–391.
- (31) Sung, W. S.; Lee, J. H.; Lee, D. G. Fungicidal Effect of Piscidin on Candida Albicans: Pore Formation in Lipid Vesicles and Activity in Fungal Membranes. *Biol. Pharm. Bull.* **2008**, *31*, 1906–1910.
- (32) Last, N. B.; Schlamadinger, D. E.; Miranker, A. D. A Common Landscape for Membrane-Active Peptides. *Protein Sci.* **2013**, 22, 870–882.

- (33) Almeida, P. F.; Pokorny, A. Mechanisms of Antimicrobial, Cytolytic, and Cell-Penetrating Peptides: From Kinetics to Thermodynamics. *Biochemistry* **2009**, *48*, 8083–8093.
- (34) Mason, A. J.; Leborgne, C.; Moulay, G.; Martinez, A.; Danos, O.; Bechinger, B.; Kichler, A. Optimising Histidine Rich Peptides for Efficient DNA Delivery in the Presence of Serum. *J. Controlled Release* **2007**, *118*, 95–104.
- (35) Sun, B. J.; Xie, H. X.; Song, Y.; Nie, P. Gene Structure of an Antimicrobial Peptide from Mandarin Fish, Siniperca Chuatsi (Basilewsky), Suggests That Moronecidins and Pleurocidins Belong in One Family: The Piscidins. *J. Fish Dis.* **2007**, *30*, 335–343.
- (36) Patrzykat, A.; Friedrich, C. L.; Zhang, L.; Mendoza, V.; Hancock, R. E. Sublethal Concentrations of Pleurocidin-Derived Antimicrobial Peptides Inhibit Macromolecular Synthesis in Escherichia Coli. *Antimicrob. Agents Chemother.* **2002**, *46*, 605–614.
- (37) Chekmenev, E. Y.; Jones, S. M.; Nikolayeva, Y. N.; Vollmar, B. S.; Wagner, T. J.; Gor'kov, P. L.; Brey, W. W.; Manion, M. N.; Daugherty, K. C.; Cotten, M. High-Field NMR Studies of Molecular Recognition and Structure-Function Relationships in Antimicrobial Piscidins at the Water-Lipid Bilayer Interface. *J. Am. Chem. Soc.* **2006**, *128*, 5308–5309.
- (38) Tran, D.; Tran, P.; Roberts, K.; Osapay, G.; Schaal, J.; Ouellette, A.; Selsted, M. E. Microbicidal Properties and Cytocidal Selectivity of Rhesus Macaque Theta Defensins. *Antimicrob. Agents Chemother.* **2008**, *52*, 944–953.
- (39) Lan, Y.; Ye, Y.; Kozlowska, J.; Lam, J. K.; Drake, A. F.; Mason, A. J. Structural Contributions to the Intracellular Targeting Strategies of Antimicrobial Peptides. *Biochim. Biophys. Acta, Biomembr.* **2010**, *1798*, 1934–1943.
- (40) Lee, C. C.; Sun, Y.; Qian, S.; Huang, H. W. Transmembrane Pores Formed by Human Antimicrobial Peptide Ll-37. *Biophys. J.* **2011**, *100*, 1688–1696.
- (41) Alam, T. M.; Drobny, G. P. Solid-State NMR Studies of DNA Structure and Dynamics. *Chem. Rev.* **1991**, *91*, 1545–1590.
- (42) Seelig, J. Deuterium Magnetic Resonance:Theory and Application to Lipid Membranes. Q. Rev. Biophys. 1977, 10, 353-418.
- (43) Das, N.; Dai, J.; Hung, I.; Rajagopalan, M. R.; Zhou, H. X.; Cross, T. A. Structure of Crga, a Cell Division Structural and Regulatory Protein from Mycobacterium Tuberculosis, in Lipid Bilayers. *Proc. Natl. Acad. Sci. U. S. A.* 2015, 112, E119–26.
- (44) Kristian, S. A.; Timmer, A. M.; Liu, G. Y.; Lauth, X.; Sal-Man, N.; Rosenfeld, Y.; Shai, Y.; Gallo, R. L.; Nizet, V. Impairment of Innate Immune Killing Mechanisms by Bacteriostatic Antibiotics. *FASEB J.* **2007**, *21*, 1107–1116.
- (45) Sochacki, K. A.; Barns, K. J.; Bucki, R.; Weisshaar, J. C. Real-Time Attack on Single Escherichia Coli Cells by the Human Antimicrobial Peptide Ll-37. *Proc. Natl. Acad. Sci. U. S. A.* **2011**, 108, E77–E81.
- (46) Pathak, N.; Salas-Auvert, R.; Ruche, G.; Janna, M.-H.; McCarthy, D.; Harrison, R. G. Comparison of the Effects of Hydrophobicity, Amphiphilicity, and Alpha-Helicity on the Activities of Antimicrobial Peptides. *Proteins: Struct., Funct., Genet.* **1995**, 22, 182–186.
- (47) Chen, Y.; Guarnieri, M. T.; Vasil, A. I.; Vasil, M. L.; Mant, C. T.; Hodges, R. S. Role of Peptide Hydrophobicity in the Mechanism of Action of {Alpha}-Helical Antimicrobial Peptides. *Antimicrob. Agents Chemother.* **2007**, *51*, 1398–1406.
- (48) Yin, L. M.; Edwards, M. A.; Li, J.; Yip, C. M.; Deber, C. M. Roles of Hydrophobicity and Charge Distribution of Cationic Antimicrobial Peptides in Peptide-Membrane Interactions. *J. Biol. Chem.* **2012**, 287, 7738–7745.
- (49) Roversi, D.; Luca, V.; Aureli, S.; Park, Y.; Mangoni, M. L.; Stella, L. How Many Antimicrobial Peptide Molecules Kill a Bacterium? The Case of Pmap-23. ACS Chem. Biol. 2014, 9, 2003–2007.
- (50) Sani, M. A.; Gagne, E.; Gehman, J. D.; Whitwell, T. C.; Separovic, F. Dye-Release Assay for Investigation of Antimicrobial Peptide Activity in a Competitive Lipid Environment. *Eur. Biophys. J.* **2014**, *43*, 445–450.

- (51) Bechinger, B. Biophysical Investigations of Membrane Perturbations by Polypeptides Using Solid-State NMR Spectroscopy. *Mol. Membr. Biol.* **2000**, *17*, 135–142.
- (52) Ouellet, M.; Bernard, G.; Voyer, N.; Auger, M. Insights on the Interactions of Synthetic Amphipathic Peptides with Model Membranes as Revealed by 31p and 2h Solid-State NMR and Infrared Spectroscopies. *Biophys. J.* **2006**, *90*, 4071–4084.
- (53) Balla, M. S.; Bowie, J. H.; Separovic, F. Solid-State NMR Study of Antimicrobial Peptides from Australian Frogs in Phospholipid Membranes. *Eur. Biophys. J.* **2004**, *33*, 109–116.
- (54) Thurmond, R. L.; Dodd, S. W.; Brown, M. F. Molecular Areas of Phospholipids as Determined by ²H NMR Spectroscopy. Comparison of Phosphatidylethanolamines and Phosphatidylcholines. *Biophys. J.* **1991**, *59*, 108–113.
- (55) Lis, L. J.; McAlister, M.; Fuller, N.; Rand, R. P.; Parsegian, V. A. Interactions between Neutral Phospholipid Bilayer Membranes. *Biophys. J.* **1982**, *37*, 657–665.
- (56) Marqusee, J. A.; Dill, K. A. Solute Partitioning into Chain Molecule Interphases: Monolayers, Bilayers Membranes and Micelles. *J. Chem. Phys.* **1986**, 85, 434–444.
- (57) Mason, A. J.; Marquette, A.; Bechinger, B. Zwitterionic Phospholipids and Sterols Modulate Antimicrobial Peptide-Induced Membrane Destabilization. *Biophys. J.* **2007**, 93, 4289–4299.
- (58) Heller, W. T.; He, K.; Ludtke, S. J.; Harroun, T. A.; Huang, H. W. Effect of Changing the Size of Lipid Headgroup on Peptide Insertion into Membranes. *Biophys. J.* 1997, 73, 239–244.
- (59) Krepkiy, D.; Mihailescu, M.; Freites, J. A.; Schow, E. V.; Worcester, D. L.; Gawrisch, K.; Tobias, D. J.; White, S. H.; Swartz, K. J. Structure and Hydration of Membranes Embedded with Voltage-Sensing Domains. *Nature* **2009**, 462, 473–479.
- (60) Nguyen, L. T.; Haney, E. F.; Vogel, H. J. The Expanding Scope of Antimicrobial Peptide Structures and Their Modes of Action. *Trends Biotechnol.* **2011**, *29*, 464–472.
- (61) Haney, E. F.; Hunter, H. N.; Matsuzaki, K.; Vogel, H. J. Solution NMR Studies of Amphibian Antimicrobial Peptides: Linking Structure to Function? *Biochim. Biophys. Acta, Biomembr.* **2009**, 1788, 1639–1655
- (62) Chi, S.-W.; Kim, J.-S.; Kim, D.-H.; Lee, S.-H.; Park, Y.-H.; Han, K.-H. Solution Structure and Membrane Interaction Mode of an Antimicrobial Peptide Gaegurin 4. *Biochem. Biophys. Res. Commun.* **2007**, 352, 592–597.
- (63) Toke, O.; Bánóczi, Z.; Király, P.; Heinzmann, R.; Bürck, J.; Ulrich, A.; Hudecz, F. A Kinked Antimicrobial Peptide from Bombina Maxima. I. Three-Dimensional Structure Determined by NMR in Membrane-Mimicking Environments. *Eur. Biophys. J.* **2011**, *40*, 447–462.
- (64) Chia, B. C. S.; Carver, J. A.; Mulhern, T. D.; Bowie, J. H. Maculatin 1.1, an Anti-Microbial Peptide from the Australian Tree Frog, Litoria Genimaculata. *Eur. J. Biochem.* **2000**, *267*, 1894–1908.
- (65) Uyterhoeven, E. T.; Butler, C. H.; Ko, D.; Elmore, D. E. Investigating the Nucleic Acid Interactions and Antimicrobial Mechanism of Buforin Ii. *FEBS Lett.* **2008**, *582*, 1715–1718.
- (66) Bloomfield, V. A. DNA Condensation by Multivalent Cations. *Biopolymers* **1997**, 44, 269–82.
- (67) Chandran, P. L.; Dimitriadis, E. K.; Lisziewicz, J.; Speransky, V.; Horkay, F. DNA Nanoparticles with Core-Shell Morphology. *Soft Matter* **2014**, *10*, 7653–7660.
- (68) Gullion, T.; Schaefer, J. Detection of Weak Heteronuclear Dipolar Coupling by Rotational-Echo Double-Resonance Nuclear Magnetic Resonance. *Adv. Magn. Opt. Reson.* **1989**, *13*, 57–83.
- (69) Rohs, R.; West, S. M.; Sosinsky, A.; Liu, P.; Mann, R. S.; Honig, B. The Role of DNA Shape in Protein-DNA Recognition. *Nature* **2009**, *461*, 1248–1253.
- (70) Ray, S.; Dhaked, H. P.; Panda, D. Antimicrobial Peptide Cramp (16–33) Stalls Bacterial Cytokinesis by Inhibiting Ftsz Assembly. *Biochemistry* **2014**, *53*, 6426–6429.